The Influence of Carrier Gas on Plasma Properties and Hydrogen Peroxide Production in a Nanosecond Pulsed Plasma Discharge Generated in a Water-film Plasma Reactor

Huihui Wang, Robert J. Wandell, and Bruce R. Locke

Department of Chemical and Biomedical Engineering, FAMU-FSU College of Engineering, Florida State University, Tallahassee, FL 32310-6046, United States

ABSTRACT

The influence of carrier gas (argon and helium) on the properties of a nanosecond pulsed filamentary discharge propagating along the water surface in a water film plasma reactor, and the effects of plasma properties on the formation of hydrogen peroxide (H_2O_2) are investigated. The plasma properties, including electron density, gas temperature, and plasma volume, and the hydrogen peroxide production rate and energy yield were measured and compared in both argon and helium discharges. The results show that helium plasma is more diffusive compared with the argon plasma, and it has lower electron density and gas temperature but larger volume. The production rates and energy yields of hydrogen peroxide are only slightly higher in the helium plasma although the electron density is much lower. A simple mathematical model with time-dependent fast radical and electron quenching in a small film surrounding the plasma core and with lumped reaction kinetics for H_2O_2 formation and degradation suggests that the hydroxyl radical (·OH) concentration is approximately two times higher in the argon discharge, but the larger volume of the helium leads to about two times more total ·OH in the helium with correspondingly higher energy yields. The experimental data and model imply that the H_2O_2 energy yield may increase at lower power (or specific energy density) for both carrier gases.

KEYWORDS: nanosecond pulsed plasma, H_2O_2 production, plasma diffuseness, plasma properties

INTRODUCTION

Atmospheric pressure non-thermal plasma discharge with liquid water has recently gained significant attention because of its potential uses in chemical and nanoparticle synthesis, material surface treatment, agriculture, and medical applications [1-3]. Non-thermal plasma discharge contacting liquid water can also be applied for water treatment since the species formed during the discharge, such as the hydroxyl radical (·OH), are strong oxidants which can efficiently degrade many pollutants in waste water and ·OH formation can often be related to the more stable chemical species hydrogen peroxide, H_2O_2 [4]. The water treatment efficiency and H_2O_2 production rate of non-thermal plasma depend on operating conditions such as input power, method of power delivery, water and gas flow rates, reactor geometry, and electrode type.

In our previous work, the effects of pulse properties including the duration, frequency and input voltage and H_2O_2 production in a nanosecond pulsed plasma discharge generated in a water film plasma reactor with argon carrier gas were investigated [5]. The H_2O_2 production rate was found to increase with the discharge power, but the energy yield of H_2O_2 decreased with the discharge power when the supplied voltage was increased. This is because the energy density of the plasma channel increased with the discharge power, thus consuming a larger amount of energy in the central core of the plasma. Since most H_2O_2 is formed at and near the interface between the liquid water and plasma [6], the increase of energy density in the middle of the plasma is not effective in increasing the production of H_2O_2. In addition, H_2O_2 can be rapidly degraded at high temperature and by reactions with electrons, atomic species, and radicals, including ·OH. The specific energy density is a parameter closely related with the diffuseness of the plasma. In many previous studies, the influence of operating conditions such as carrier gas type, gas flow rate, and water concentration on the diffuseness and homogeneity of several different types of plasma were analyzed [7-9]. For many non-thermal plasma applications, especially applications in biomedicine and materials engineering, a diffusive and homogeneous discharge is preferred since it provides a uniform treatment and is capable of avoiding damage to sensitive cells and materials [10, 11]. However, the understanding of the influence of plasma diffuseness on water treatment efficiency, formation of ·OH, and H_2O_2 production is limited.

In the present study plasmas of different diffuseness were generated using argon and helium in a gas-liquid film reactor, and the plasma properties including electron density and gas

temperature and the H_2O_2 production rates and energy yields of these two different types of plasma were compared in order to investigate the mechanism of H_2O_2 formation and assess the influence of specific energy density on H_2O_2 production.

METHODS

Experimental Setup

The experimental setup, shown in Figure 1, is similar to that utilized in our previous work [12, 13]. Deionized water is delivered into the system by a reciprocating pump (Optos Series, Eldex Laboratories; Napa, CA) at a flow rate of 2 mL/min, and mixed with the high-pressure carrier gas: argon and helium (Air Gas, ultra high purity) inside a Swagelok T-joint (1/16 in [1.5875 mm], Jax Fluid System Technologies; Jacksonville, FL). The high pressure carrier gas source was set to 400 kPa and allowed to flow into the mixing zone without restriction. The water-

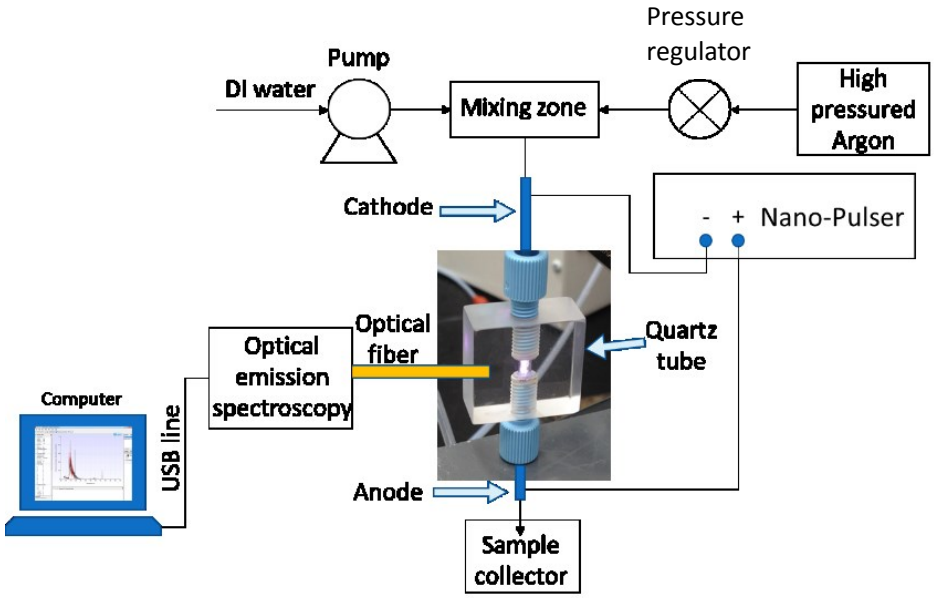

Fig 1. Experiment set up

gas mixture was introduced into the quartz reactor chamber through a capillary nozzle (I.D. = 0.254 mm), which also functions as the cathode. The flowing water forms a film along the reactor wall upon entering the discharge region. The liquid and gas exit the reactor through the lower nozzle which also functions as the anode. The carrier gas flow rate, 0.5 L/min, was measured at the exit of the lower nozzle with a bubble flow meter (Supelco, 1 L). The H_2O_2 concentration in

the outlet liquid sample was determined [14] by adding titanium sulfonate into the sample and measuring the absorption of light at 407nm wavelength with a UV-Vis spectrometer (Perkin-Elmer, Lambda 35; Waltham, MA). The concentration of H_2O_2 is proportional to the light absorption as determined by calibration with known standards. A nanosecond pulsed power supply (NSP 120-20, Eagle Harbor Technologies, LLC, Seattle Washington) was connected to the anode and cathode to provide 20 nanosecond high voltage pulses at a relatively high repetition frequency (2 kHz). The plasma discharge was generated along the water film inside the reactor as in our previous work [15]. An optical emission spectrometer (Avantes, AvaSpec-ULS3848) with resolution 0.1 nm was coupled with an optical fiber to collect the emission during the plasma discharge. The plasma properties including gas temperature and electron density were measured by analyzing the spectrum as described in a following section. All the measurements including the power and the H_2O_2 production rate and energy yield were repeated three times under each operational setting, and the error bars are based upon one standard deviation.

Power Measurement

Electrical analysis was performed with an oscilloscope (Tekronix MDO 3014; Beaverton, OR) coupled with two high voltage probes (TektronixP6015A, 1/1000; Beaverton, OR) and a Rogowski coil (Pearson Electronics, model 6585; Palo Alto, CA). The non-differential high voltage probes were connected together at the grounds to generate a floating reference while the high voltage tips were connected to the anode and cathode. The values from these two probes were added together to measure the total electrical potential across the electrode gap. The Rogowski coil was placed around discharge gap to measure the current flow only through the discharge region. Placement of the Rogowski coil in this manner minimizes in inclusion of capacitive current in the waveforms. The minimization of capacitive current can be seen in Figure 2 which compares placement of the Rogowski coil around the HV lead (left) with placement around the discharge gap (right) at an output voltage of the 2 kV on the nanopulser. The left waveform clearly shows a simultaneous rise in current with voltage related to capacitive charging of the electrodes, however, the right waveform where, the Rogowski is centered around the discharge gap, shows little to no

Fig 2. Left: 2 kV discharge with Rogowski coil placed around HV lead. Right: 2 kV discharge with the Rogowski coil centered on the plasma discharge region. The 2 kV output voltage was insufficient to generate a plasma discharge. Comparison of these two waveforms illustrates the minimization of capacitive current when the Rogowski coil is centered on the discharge region.

measured current because the 2 kV output voltage setting in insufficient to generate a plasma discharge.

To ensure proper temporal alignment of the two high voltage probes with the Rogowski coil, the nanopulser was discharged across a resistor where current should rise simultaneously as a voltage is applied. In this case the HV probes were connected to each end of the resistor which was also centered inside the Rogowski coil. The offset (deskew) of each high voltage probe was

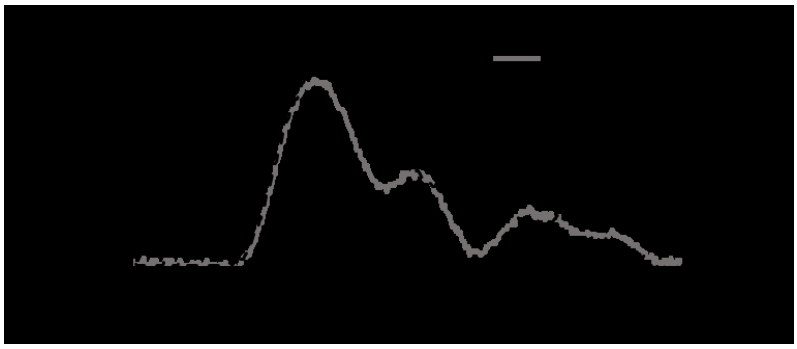

Fig 3. Discharge across a resistor for temporal alignment of the two high voltage probes with the Rogowski coil. Output voltage setting on the nanopulser was 2kV.

adjusted on the oscilloscope until alignment was achieved. This calibration is shown in Figure 3.

The energy consumed in each pulse was calculated by Equation (1).

$$\text{Energy per pulse} = \int V(t)I(t)dt \tag{1}$$

where I and V are current and voltage, respectively. To calculate the mean discharge power the energy consumed in each pulse was multiplied by the pulse repetition frequency.

Gas temperature measurement

1. N_2 (C-B): The spectrum of N_2 (C-B; 0-0) near 337 nm was used for determination of the gas temperature by measurement of the rotational temperature of nitrogen [16]. In order to generate the N_2 (C-B) emission, 200 ppm of nitrogen was introduced into the system and mixed with argon. For plasma generated in helium, the emission of nitrogen was caused by impurities in the helium tank. Specair was used to fit the experimental spectrum to determine the gas temperature [17].

2. OH (A-X) two temperature fitting: The rotational temperature of ·OH has also been proven to be a good estimation of the temperature in some plasmas [16]. However, the rotational population of ·OH may deviate from the Boltzmann distribution when a large amount of water exists in the system [18]. Therefore, temperatures measured by OH (A-X) emission when assuming the ·OH obey the Boltzmann distribution can lead to an overestimation. One way to address this issue is by fitting the Boltzmann plot with multiple straight lines each with different slope and corresponding to different temperatures. The temperature corresponds to the lower rotational states where $N' < N'_{max}$ has been proven to be a good estimate of the gas temperature. However, by using this method, the fitting results mostly depend on the arbitrarily chosen value of N'_{max}, which makes the determination of gas temperature less certain [19].

In order to avoid such problem, another method developed by Vorac et al.[19] was used to fit the experimental distribution to the sum of two independent Boltzmann distributions. The distribution model is a function of rotational temperature for both the cold and hot groups. The two temperatures were found simultaneously by minimizing the expression

$$\min_{(a_1, a_2, T_1, T_2)} \sum_{(J',N')} \left[ln\left(a_1 e^{-E_{(J',N')}/(kT_1)} + a_2 e^{-E_{(J',N')}/(kT_2)} \right) - ln\left(\frac{n_{(J',N')}}{2J'+1} \right) \right]^2 \qquad (2)$$

where a_1 and a_2 are the linear factors for the cold and hot group respectively. T_1 and T_2 are rotational temperature of the respective groups. The rotational temperature of the cold group was considered close to the gas temperature as previously reported [16, 19].

Electron density measurement

An initial order of magnitude estimation of electron density from the current density gives 10^{15} cm^{-3} and 10^{16} cm^{-3} for helium and argon plasmas, respectively. For both the helium and argon plasma, the electron density was measured using the Stark broadening of the H_α line located at 656.3 nm from a temporally and spatially averaged spectrum.

The H_α line was first deconvoluted into the Gaussian and Lorentz profiles by fitting the H_α peak to the Voigt function. The FWHM of Stark broadening was then determined by subtracting the contribution of van der Waals broadening from the total FWHM of Lorentzian profile, and the electron density was then estimated through Equation (3) [7].

$$FWHM = 1.78\,nm \times \left(\frac{n_e}{10^{23} m^{-3}}\right)^{0.67965} \tag{3}$$

Where $FWHW$ is the full width at half maximum of the Stark profile.

Estimation of plasma volume and liquid-plasma contact area

The maximum cross-sectional area of the plasma channel was estimated from the current density model [20] as described by Equation (4) using the peak current and the electron density measured by the time and space averaged spectrum [20].

$$A = \frac{I}{J} = \frac{I}{n_e e \mu_e E} \tag{4}$$

where n_e (cm^{-3}) is electron density, J ($A.cm^{-2}$) is current density, I (A) is the maximum discharge current, A (cm^2) is the correlated maximum cross-section areas of plasma channel, e (C) is

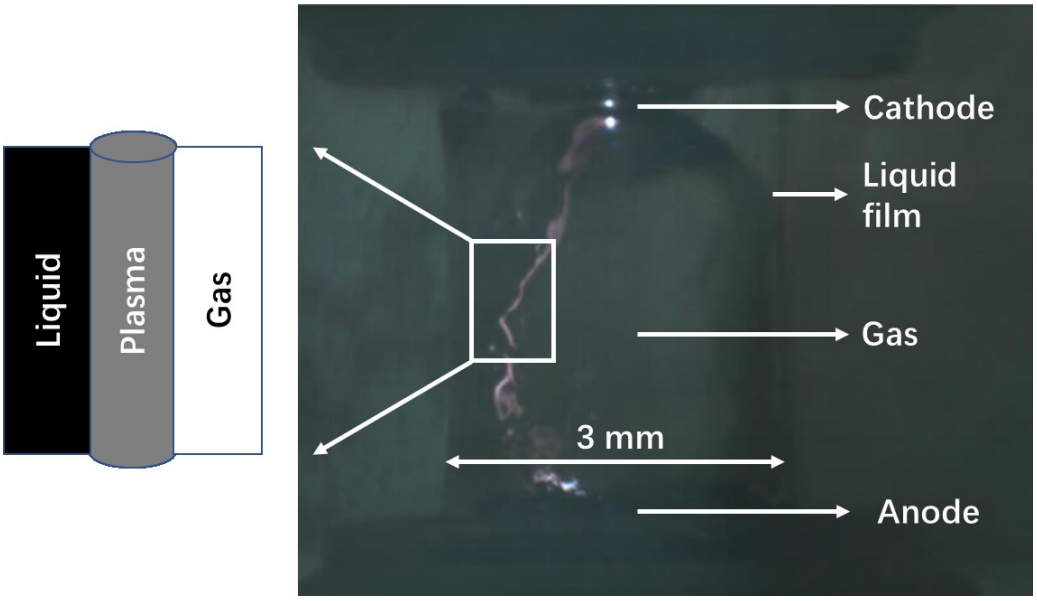

Fig 4. Image of discharge in argon. The power settings were fixed at 18 kV, 20 ns, and 2 kHz. The shutter speed and frame rate of high speed camera were set to 1/8000 and 4000 separately to capture a single pulse.

elementary charge of electron, E (V/cm) is the electric field estimated by dividing the breakdown voltage by the gap distance, μ_e ($cm^2.(V.s)^{-1}$) is the electron mobility estimated using Bolsigplus [21]. According to the image of the discharge shown in Figure 4, a filamentary plasma channel forms and propagates along the liquid-gas interface. The length of the plasma channel approximately equals the electrode gap distance, i.e., the length of the discharge region. Therefore, the volume of the plasma channel was approximated by the length of the electrode gap (0.4 cm) multiplied by the cross-sectional area of the plasma channel. Because the maximum discharge current was utilized for this calculation, the plasma volume estimated using this method likely corresponds to the maximum volume during the pulse. The maximum plasma-liquid contact area was estimated by assuming the plasma channel to be cylindrical, and only half of the cylinder surface contacts the liquid since the plasma channel forms at the interface between the gas and liquid phases as shown in Figure 4. This approximate method illustrates the trends of the plasma volume and plasma-liquid contact area variation with different voltage settings (discharge powers).

RESULTS AND DISCUSSION

Electrical diagnosis

Figure 5 shows the increase of discharge power with the voltage setting for both the argon and helium plasmas where the pulse width and pulse frequency were fixed at 20 ns and 2 kHz, respectively. The total discharge power of the helium plasma is slightly higher than that of the argon plasma at the low voltage setting, but they are about the same at 18 kV. The current and voltage waveforms for both the helium and argon plasmas have similar shapes, and the peak current is the same for both gases. However, the breakdown voltage is lower in the helium plasma. A lower breakdown voltage in helium discharges was also observed in other studies [22, 23]. Investigation of electrical breakdown over a liquid water surface is very limited, and future work is needed to develop a theory to describe electrical breakdown in cases where the nanosecond pulsed plasma moves along the interface between a liquid water and gas.

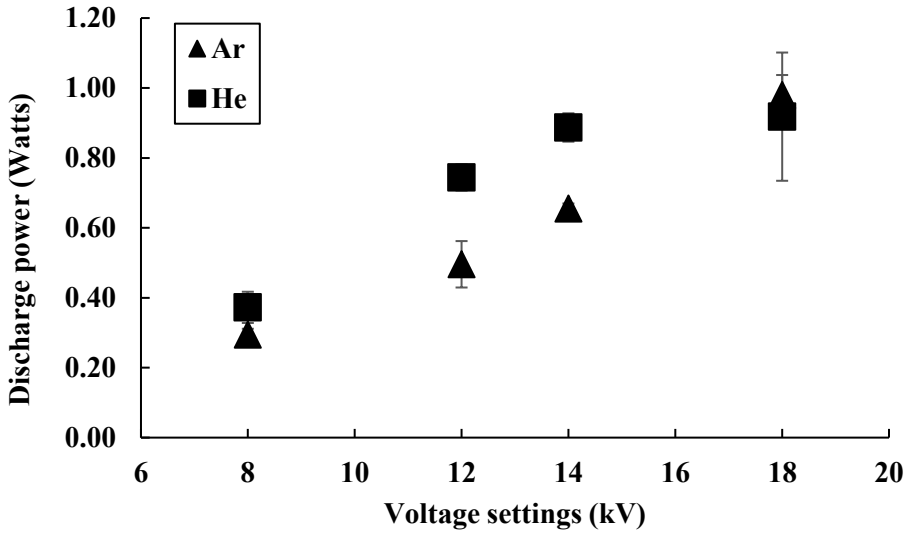

Fig 5. The increase of discharge power with power supply voltage setting: frequency and pulse width were fixed at 2 kHz and 20 ns, respectively. Liquid flow rate was 2 mL/min. Where not observable the error bars are within the symbols.

Plasma properties under different power settings

Figure 6 shows the Boltzmann plot generated using MassiveOES [19] and the two temperature fitting curves for the helium plasma at 12 kV. The Boltzmann plot clearly shows that

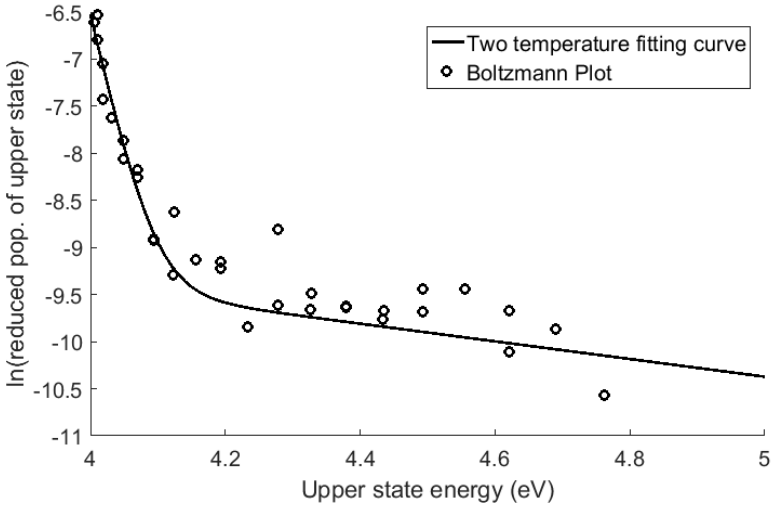

Fig 6. Boltzmann plot of OH (A-X) peak in helium plasma at the power setting of 12 kV, 20 ns, and 2 kHz. The liquid flow rate was set to 2 mL/min in this case.

the population distribution of ·OH deviates from the Boltzmann distribution in the system due to the presence of a large amount of water, and the distribution can be fitted by two temperature groups, one with a high temperature and another with a low temperature. In the case shown in Figure 6, the cold group temperature is 365.1 K, and the hot group temperature is 4350 K. This result again suggests the overpopulation of ·OH at the high rotational states. Figure 7 shows the spectrum fitting of the N_2 (C-B) peak conducted using Specair [17]. The gas temperature of the plasma was determined with Specair through the spectrum fitting. According to Figure 8, the temperature measured by the two-temperature fitting method is very consistent with the temperature measured by the spectrum fitting of the N_2 (C-B) peak for all discharge powers. The

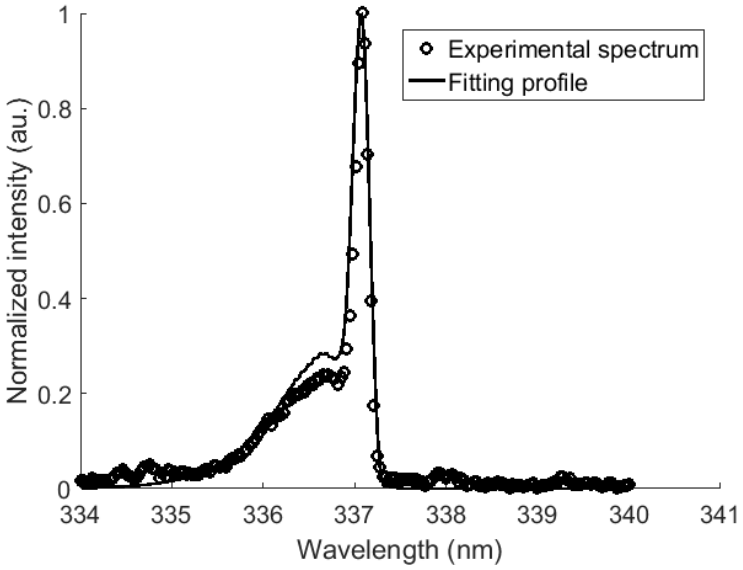

Fig 7. Spectrum fitting of N2 (C-B) peak at 12 kV, 20 ns, and 2 kHz for helium discharge. The liquid flow rate was set to 2 mL/min. The rotational temperature was found to be 358 K in this case.

error bars for the gas temperatures measured using the N_2 (C-B) peak are very small and the larger error bars of the temperature measured by the two-temperature fitting method are probably caused by the inconsistency of the background removal before each spectrum was fit.

As shown in Figure 8, the gas temperature is approximately two times larger in the argon plasma than in the helium plasma. Wang et al.[24] reported a similar result in a dry atmospheric microplasma discharge using both experiments and simulations. In that work, they concluded that convective heat dissipation plays a more important role in the argon discharge and that conductive heat loss is more important in the helium discharge due to the different thermal conductivities of

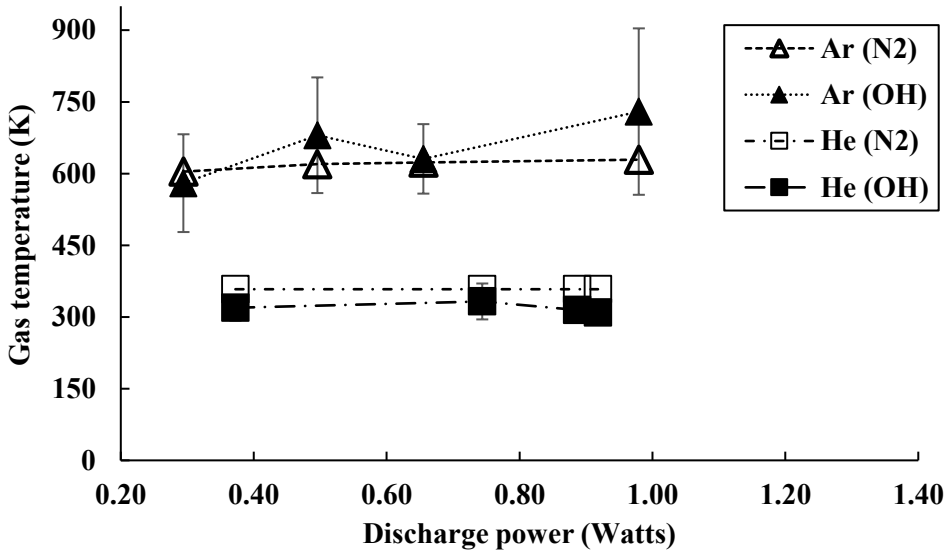

Fig 8. Gas temperature of plasma measured by different methods. The pulse duration and frequency were fixed at 20 ns and 2 kHz respectively, and the discharge power was changed by adjusting the voltage settings. The liquid flow rate was set to 2 mL/min. Where not observable, the error bars are within the symbols.

the two gases. Figure 8 also shows that the temperature does not change significantly with increasing voltage setting (or discharge power) for both the argon and helium plasmas, which shows that gas heating was not significantly influenced by the discharge power.

Figure 9 shows examples of the H_α peak fitting for both the argon and helium plasmas at 18 kV. The peak profile for the argon plasma is much broader than that for the helium plasma, and this suggests a higher electron density in the argon plasma. As shown in Figure 10, the electron

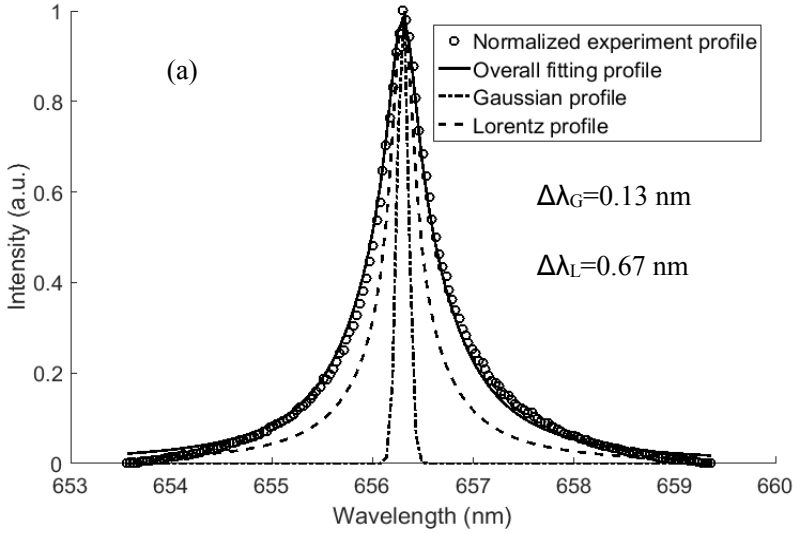

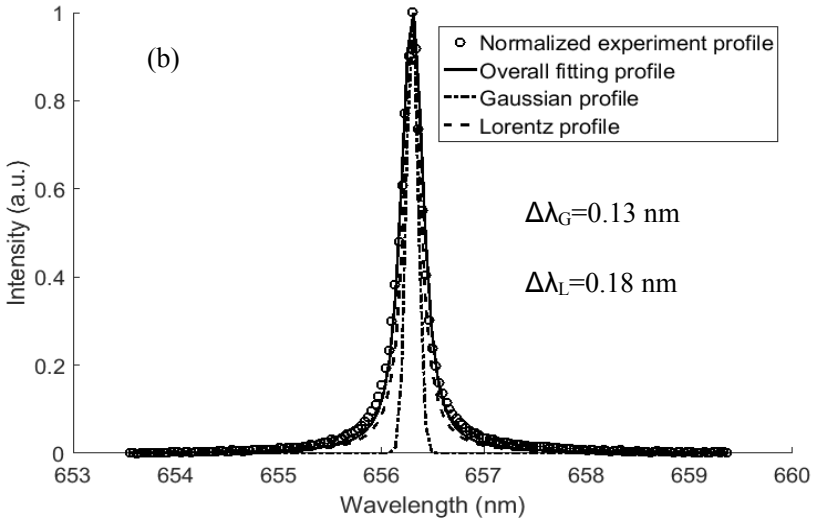

Fig 9. Profile fitting of H_α peak in (a) argon and (b) helium plasmas. The voltage setting, pulse duration and frequency were fixed at 18 kV, 20 ns, and 2 kHz respectively in both cases.

densities of the argon plasma are approximately one order of magnitude larger than those in the helium plasma, and the electron density increases with the discharge power adjusted by changing the voltage setting in both helium and argon plasmas. However, the electron density increases proportionally more steeply with discharge power in helium than in argon. The electron density of

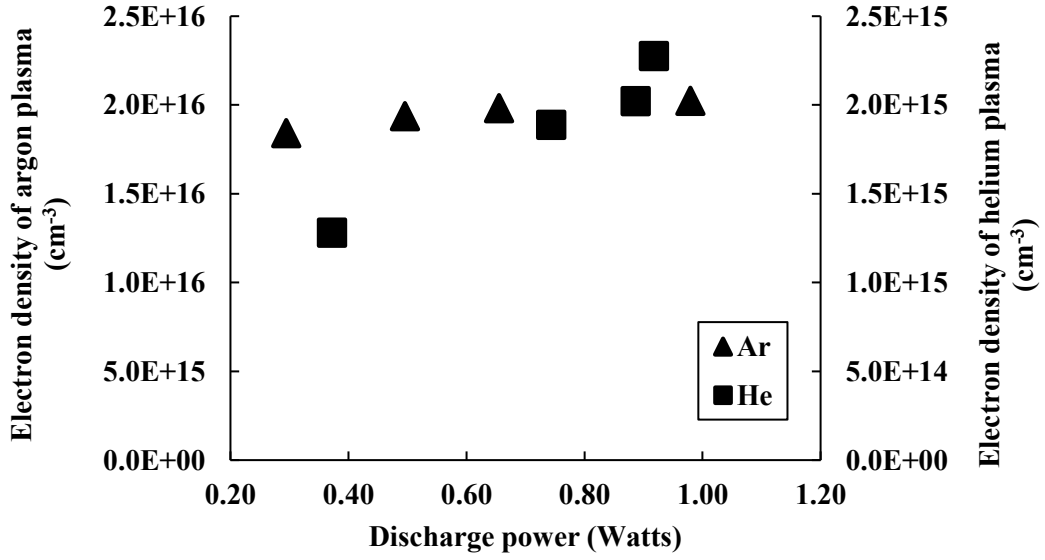

Fig 10. Average electron density over time and space for different discharge powers. The pulse duration and pulse frequency were fixed at 20 ns and 2 kHz respectively, and the discharge power was changed by adjusting the voltage settings of the power supply. Liquid flow rate was set to 2 mL/min in each case. The error bars are within the size of the symbols.

helium increases about 70% between 0.37 W and 0.92 W, while in the argon plasma it only increases about 10% between 0.29 and 0.98 W. The increase of electron density in both cases is due to the increase of the plasma specific energy density as the discharge power was increased. The less significant increase of electron density in the argon plasma indicates that the energy was not as efficiently used to generate free electrons as the discharge power was increased. The lower temperature and electron density of the helium plasma in our work indicate a larger diffuseness of the helium plasma compared to argon. Further consideration of the diffuseness of the plasma will be discussed in the following section.

Diffuseness of plasma generated in argon and helium

One important reason for the different diffusive properties of plasma are the different time scales for ion-electron dissociative recombination and diffusion. The mobility of ions in helium is generally about one order of magnitude larger than in argon [25], which implies larger diffusion rates in the helium plasma. The ambipolar diffusion coefficient can be estimated by Equation (5) [26].

$$D_a = \frac{\mu_i k T_e}{e} \tag{5}$$

In Equation (5), μ_i is the ion mobility, T_e is the electron temperature which is assumed to be 4 eV based on other work [5] (and the other similar work [27-29] give the value of electron temperature from 3 eV to 5 eV), k is Boltzmann's constant, and e is the elementary charge of the electron. Table 1 shows the timescales for Ar_2^+ and He_2^+reactions and diffusion and the length scale for diffusion in the plasma determined using the equations as listed in the table. $D_{reactor}$, k_{ei}, and t_{diss} in Table 1 are the diameter of the reactor, the reaction rate coefficient of electron-ion dissociative recombination, and the diffusion time scale, respectively. The residence times of the liquid phase and gas phase in the water film reactor are 150 ms and 2.5 ms [5], respectively, and both are much longer than the time scales of the reactions and the pulse duration (i.e., 20 ns). Therefore, both the gas phase and liquid phase can be viewed as stationary compared to the pulse. The residence time was determined by dividing the volume of liquid phase and gas phase in the reactor, respectively, by the volumetric flowrate. The volumes of liquid and gas were estimated from high speed imaging.

The timescales required for diffusion through the entire reactor (t_{CDiff}) in argon and helium are about 7 ms and 1.3 ms, respectively, and are both much longer than the reaction timescales as well as the time scale of the pulses. This suggests that the fast electron-ion dissociative recombination in argon and helium plasmas prevent diffusion throughout the entire reactor, and therefore a filamentary plasma channel is formed as shown in Figure 4. However, a more diffusive plasma is likely formed in helium since the diffusion length scale in the helium discharge is much larger than the diffusion length scale in the argon discharge because of the higher diffusion coefficients and smaller reaction rate coefficients of ions in helium. These estimates support the observation of the more diffuse nature of the helium plasma compared to the argon case.

Table 1. Time and length scale of diffusion and reactions in argon and helium plasmas

Reactions	$k_{ie\ [30,\ 31]}$ (cm^3/s)	n_e (cm^{-3})	$t_{diss}(s)=1/(k_{ie}*n_e)$	$t_{Cdiff}(s)=D_{reactor}^2/2D_a$	$L_{diff}[3]=(2D_a*t_{diss})^{0.5}$
$Ar_2^+ + e = Ar + Ar$	1.94×10^{-8}	1.00×10^{16}	5.16×10^{-9}	7.00×10^{-3}	2.58×10^{-4}
$He_2^+ + e = He + He$	1.10×10^{-12}	1.00×10^{15}	9.08×10^{-4}	1.27×10^{-3}	2.54×10^{-1}

A model based upon the electron density and discharge current [20], given in Equation (4), was used to estimate the plasma volumes with variation of carrier gas and discharge power as shown in Figure 11. This current density model provides an estimation of the maximum plasma volume and is useful for comparing the relative volumes for the two different gases. The estimated volume of the helium plasma is about one order of magnitude larger than the volume of the argon plasma. This result is also consistent with the highly diffuse nature of the helium plasma. In addition, this result shows that the volumes of the plasmas generated in argon and helium both increase with discharge power. The volume of the argon plasma increased about 4 times from 0.29 W to 0.98 W, while the volume of the helium plasma expanded only about 70% from 0.37 W to 0.92 W.

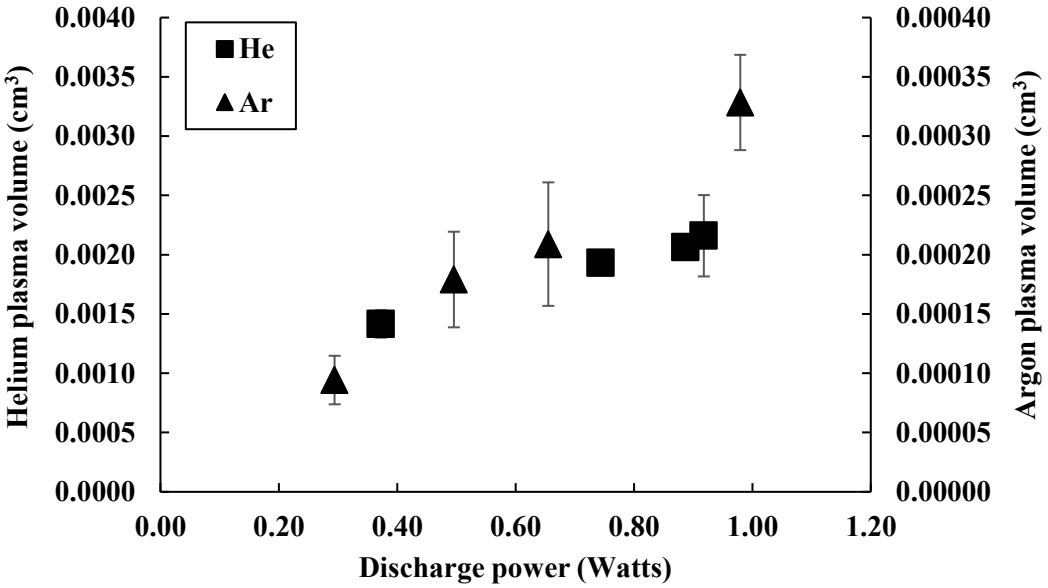

Fig 11. Plasma volume estimated using current density model under different discharge power. The pulse duration and pulse frequency were fixed at 20 ns and 2 kHz respectively, and the discharge power was changed by adjusting the voltage settings. Liquid flow rate was set to 2 mL/min in each case. Error bars are within the size of the symbols where not observable.

Figure 12 shows the electron density and temperature of the plasmas generated in a range of helium-argon mixtures. Both the electron density and gas temperature decrease with increasing helium percentage, and this result is due to the changing diffusion and reaction properties as the proportion of helium becomes larger. The decrease of electron density is very small with increasing helium at the lower percentage levels, but when the helium percentage exceed 70% the drop was much larger. The ion mobility in a gas mixture increases as helium is added to argon according to Blanc's law [32] given in Equation 6.

$$\frac{1}{\mu} = \frac{f_1}{\mu_1} + \frac{f_2}{\mu_2} \tag{6}$$

In the above equation, μ is the mobility of ions in the gas mixture, μ_i is the mobility of ions in the pure gas, and f_i is the fraction of different types of gases in the mixture.

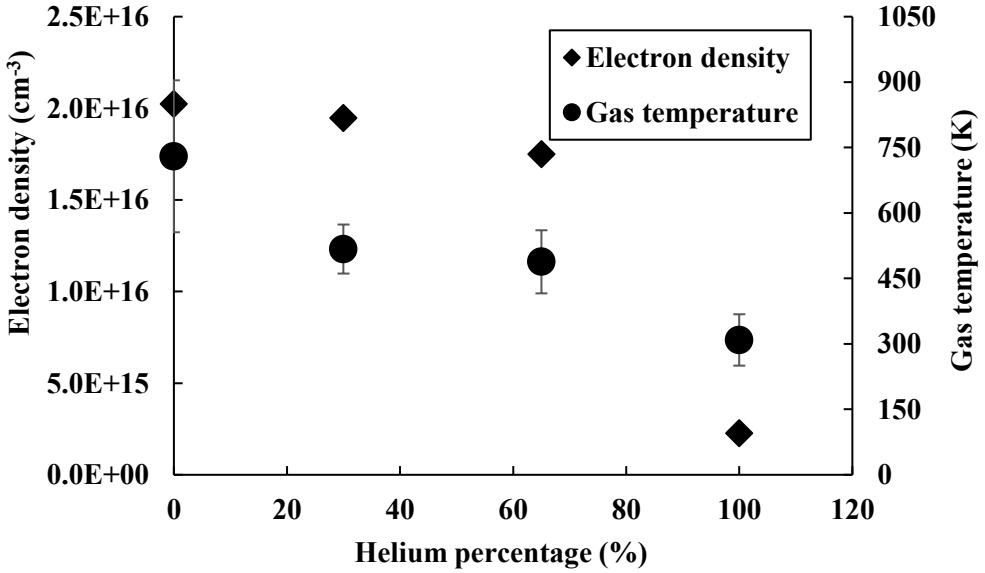

Fig 12. Electron density and gas temperature with different helium percentages. The gas temperature was measured using OH (A-X) peak and two temperature fitting method. The voltage, pulse duration, and pulse frequency were set to 18 kV, 20 ns, and 2 kHz respectively. Liquid flow rate was 2mL/min. The error bars for the electron density are within the symbols.

Equation (6), with the pure species ion mobility data from the literature [25], shows that the ion mobility in the gas mixture increases with increasing helium percentage as shown in Figure 13. The increase is small at low helium concentration and becomes larger at high helium concentration. This result is consistent with the nonlinear decrease of electron density with helium

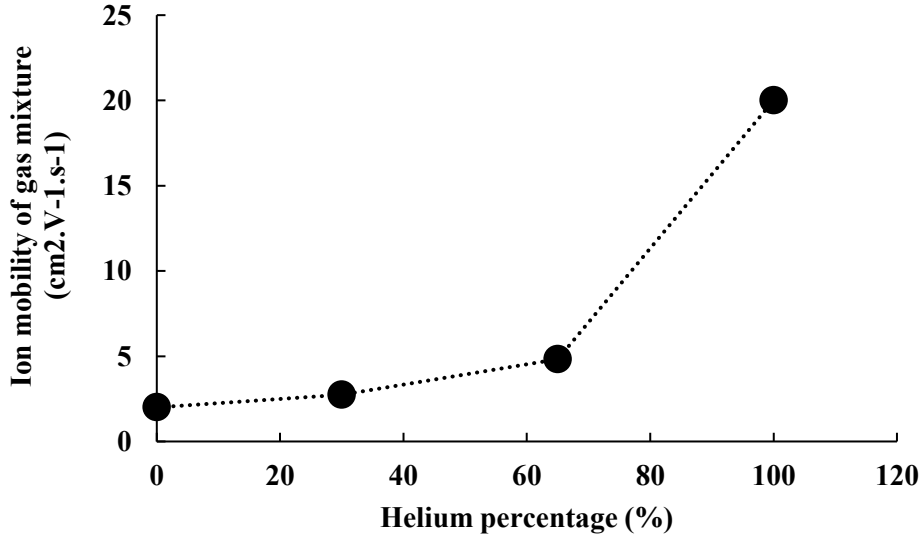

Fig 13. Ion mobility in helium-argon mixtures with helium percentage according to Equation (6).

percentage shown in Figure 12. Because ion mobility increases very slowly at low helium percentages, the plasma volume and diffuseness only change slightly, therefore the electron density also decreases slowly in this range. Gas temperature additionally drops with increasing helium percentage. This is probably because the concentration of electrons was 'diluted' by adding helium into argon, therefore the gas heating process through the electron-molecule collisions was also reduced and as a result the gas temperature decreased with the helium percentage.

H_2O_2 production and energy yield

Figure 14 shows the H_2O_2 production rate and the energy yield for both argon and helium plasmas under the different discharge power. The production rate of H_2O_2 is slightly higher in the helium plasma, and it increased with discharge power in both argon and helium plasmas. The production rate of H_2O_2 is influenced by the concentration of ·OH since most of the H_2O_2 is formed by recombination of ·OH [4, 30, 31]. The electron density affects the rate of dissociation of water, therefore influencing the generation of ·OH. The ·OH, other atomic and radical species, and

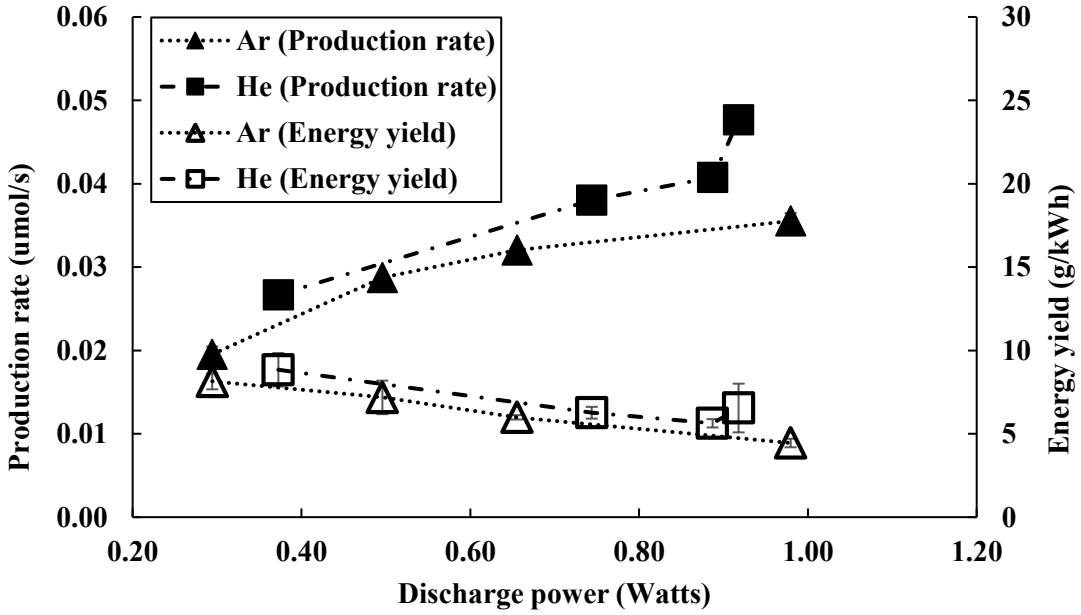

Fig 14. Energy yield and production rate of H_2O_2 in both argon and helium plasmas with different discharge power. The pulse duration and pulse frequency were fixed at 20 ns and 2 kHz, respectively, and the discharge power was changed by adjusting the voltage setting of the power supply. Liquid flow rate was fixed at 2 mL/min. Error bars are within the symbols where not observable.

electrons affect the degradation rates of H_2O_2 as well. However, the overall H_2O_2 production rate increased with the electron density as the discharge power increased in both cases. This result is consistent with the result found in other studies where a higher electron density resulted in a higher H_2O_2 concentration [9]. The energy yield, however, decreases with the discharge power in both plasmas as shown in Figure 14. This suggests that the power was less efficiently used to produce H_2O_2 as the discharge power was increased by changing the voltage setting. According to Figure 5 and Figure 10, the discharge power increased about 4 times as the voltage setting was changed from 8 kV to 18 kV, but the electron density only increased 10 percent and 70 percent in the argon and helium plasmas, respectively, thus suggesting a lower efficiency in electron formation. In addition, as the volume of the plasma channel increases a larger amount of energy is needed to increase the specific energy density of the plasma. However, the specific energy density increase in the center core of the plasma channel would not significantly affect the H_2O_2 production because most of the H_2O_2 is formed at the plasma-water interface as suggested by our previous study [33]. A more detailed analysis will be shown using a simple mathematical model in the following section.

The production rate of H_2O_2 in the argon plasma is slightly lower than in helium even though the electron density of the argon plasma is one order of magnitude higher. This suggests that the relationships between H_2O_2 production rate and factors other than electron density also need to be considered. The correlation tests among discharge power, electron density, area of plasma-liquid interface, and H_2O_2 production rate suggests that the plasma properties, including the electron density and the area of the plasma-liquid interface, are both positively and linearly correlated with both the discharge power and the H_2O_2 production rate in the argon and helium plasmas. The interface between the plasma and the liquid plays an important role in ·OH recombination and H_2O_2 formation since most of the H_2O_2 collected in the liquid sample is formed at or in the plasma-liquid interface. This is because H_2O_2 rapidly dissociates under the influence of elevated temperature, high ·OH and other radical concentrations, and large electron density in the core of the plasma channel. However, the gas temperature, ·OH concentration, and electron density decrease dramatically at the interface between the plasma and liquid phases due to quenching and cooling by the convection and evaporation of water [34]. This quenching suppresses the degradation of H_2O_2 at the boundary of the plasma. Further, in the nanosecond pulses used here,

the time scale for plasma decay is very fast leading to significant temporal quenching. Since the helium plasma is more diffusive, and the plasma volume is larger, the contacting region between liquid and plasma is also larger in the helium plasma than in the argon plasma. In order to compare the mechanism of H_2O_2 formation in argon and helium plasmas and investigate the importance of plasma volume to the H_2O_2 production, a simple reaction model was developed as described in Appendix I. The model describes reactions in a thin film region at the boundary of the plasma with the liquid and includes H_2O_2 formation by ·OH (reactions 1 or 2 in Table 2) and destruction (reactions 3 to 10 in Table 2). The reaction rates are dependent on the electron density, electron temperature, and gas temperature as indicated in the table. The gas temperature and electron density were taken from the experimental measurements. Since the model is not very sensitive to the electron temperature, we assumed the electron temperature equals 4 eV [5].

Table 2. Reaction coefficients for the major reactions with H_2O_2 and OH involved [9]

No.	Reaction	Rate coefficient k	k in helium at 358 K	k in argon at 600 K	Ref
1	$OH + OH + Ar \rightarrow H_2O_2 + Ar$	$6.9 \times 10^{-43}(T_g/300)^{-0.8}$		3.96×10^{-43}	[35]
2	$OH + OH + He \rightarrow H_2O_2 + He$	$3.7 \times 10^{-43}(T_g/300)^{-0.8}$	3.21×10^{-43}		[36]
3	$H + H_2O_2 \rightarrow HO_2 + H_2$	$2.81 \times 10^{-18} exp(-1890/T_g)$	1.17×10^{-19}	8.70×10^{-19}	[37]
4	$H + H_2O_2 \rightarrow H_2O + OH$	$1.69 \times 10^{-17} exp(-1780/T_g)$	1.43×10^{-20}	1.20×10^{-19}	[38]
5	$O + H_2O_2 \rightarrow HO_2 + OH$	$1.4 \times 10^{-18} exp(-2000/T_g)$	5.25×10^{-21}	4.99×10^{-20}	[38]
6	$OH + H_2O_2 \rightarrow H_2O + HO_2$	$2.91 \times 10^{-18} exp(-160/T_g)$	1.86×10^{-18}	2.23×10^{-18}	[37]
7	$e + H_2O_2 \rightarrow H_2O + O^-$	$1.57\ x10^{-16}\ T_e^{-0.55}$			[39]
8	$e + H_2O_2 \rightarrow OH + OH^-$	$2.7x10^{-16}\ T_e^{-0.5}$			[39]
9	$e + H_2O_2 \rightarrow 2OH + e$	$1x10^{-9}$			[40]
10	$e + H_2O_2 \rightarrow H + HO_2 + e$	$1x10^{-9}$			[40]

Figure 15 shows the ·OH concentrations in a single pulse for argon and helium as functions of input power determined by fitting the model to the experimental data as described in Appendix I. Averaging the ·OH concentrations from Figure 15 by multiping by the pulse width and frequency gives values of 3.92 $x10^{14}$ cm^{-3} to 4.82 $x10^{14}$ and 1.98 $x10^{14}$ to 2.40 $x10^{14}$ cm^{-3}, respectively, in

argon and helium, respectively. The averaged ·OH concentrations estimated by this method for the argon plasma are lower than the ·OH concentration of 4 x10^{16} cm^{-3} which we measured in a higher power (1 to 2 W) microsecond discharge using chemical probes in the same reactor under the same gas and liquid flow conditions as in the present study [33]. Our values are higher than those estimated by Du et al. for water vapor plasma in argon and helium at higher powers, i.e. 4x10^{13} cm^{-3} and 8x10^{13} cm^{-3} at 0.9W and 2.4% water vapor. Li et al. found, using laser-induced fluorescence (LIF) spectroscopy, values of ·OH concentration of 10^{15} cm^{-3} and 10^{13} cm^{-3} for argon and helium, respectively, in a micro-discharge surface plasma with water vapor where plasma temperatuers were in the range of 300 to 350 K and electron energy was approximately 5 eV [28].

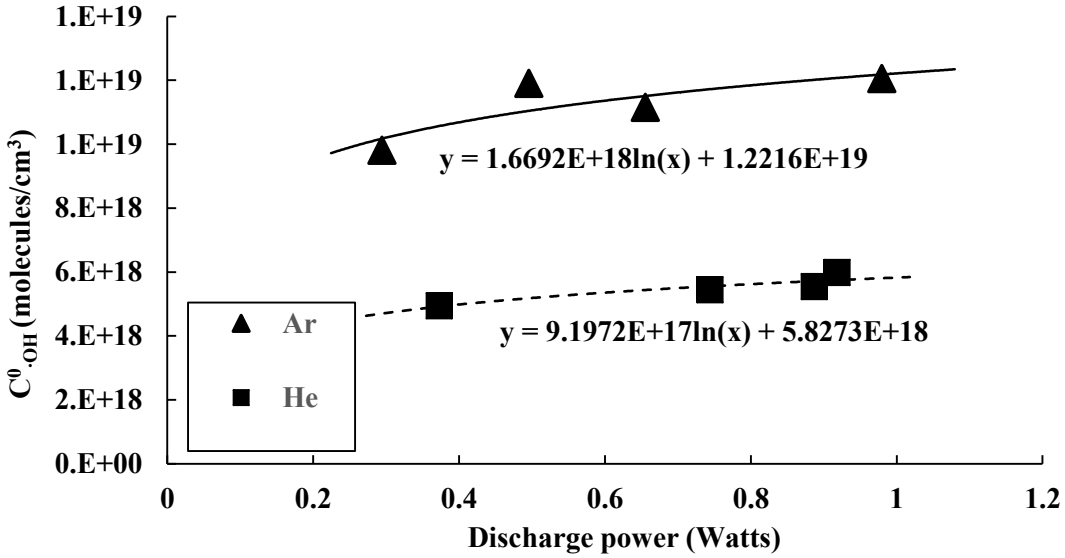

Fig 15. Concentrations of ·OH for helium and argon during a single pulse obtained from the reaction model described in Appendix I. The error bars are within the size of the symbols due to the small variation of model input parameters.

A variety of LIF measurements of ·OH in various types of plasmas including dielectric barrier discharge, radio frequency glow and jets, pulsed streamer discharge, pulsed jet, and pulsed dielectric barrier for heium and argon plasmas with water vapor were summarized and values of ·OH ranged between 10^{13} to 10^{15} cm^{-3} [28, 41]. Perhaps closest to our work is a nanosecond (3.7 mJ/pulse) pulsed discharge formed at a liquid water interface with an argon carrier where the ·OH concentration, found by LIF, was approximately 3x10^{14} cm^{-3} and values up to 2 x10^{15} cm^{-3} were predicted based upon kinetic modeling [42]. Values of ·OH as high as 10^{16} cm^{-3} based upon LIF and a chemical model have been reported for helium-water vapor nanosecond pulsed filamentary

discharges with electron densities in the range of 10^{15} to 10^{16} cm^{-3} and a gas temperature of 600 K [43].

The concentration of ·OH is only two times larger in the argon plasma than in the helium plasma even though the electron density is one order of magnitude larger in the argon plasma. This suggests that the ·OH generation is less efficient in the argon discharge. Further, the concentration

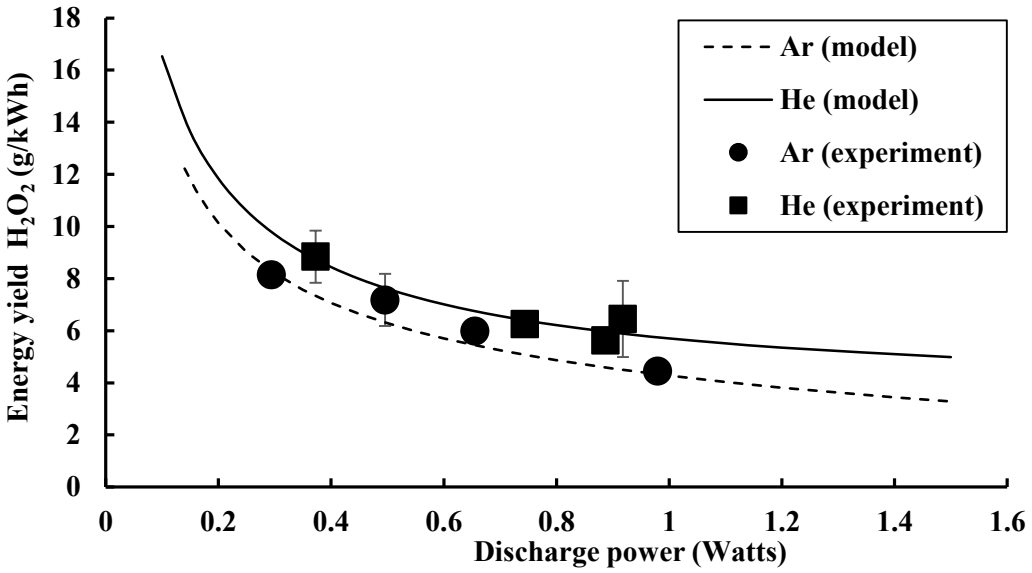

Fig 16. H_2O_2 energy yields experimental data compared to the model: Energy yield vs discharge power. Improvements in energy yield are predicted to occur at lower dishcarge power. Where not observable, the error bars are within the size of the symbols.

of ·OH increased only about 20% in both plasmas when discharge power was increased from 0.29 to 0.98 W for the argon plasma and 0.37 to 0.92 W for the helium plasma. The decrease in efficiency for ·OH generation in both plasmas as the discharge power was increased explains the decrease of energy yield with discharge power as shown in Figure 16. Utilizing the power dependencies of electron density, gas temperature (for argon), radius of plasma channel, and $C_{\cdot OH}{}^{0}$, we extrapolated the model in order to show the trends in H_2O_2 energy yield with discharge power. Figure 16 shows that as the power increases from the experimentally measured range, the H_2O_2 energy yields for both gases decrease while the energy yields for both gases increase with decreasing discharge power. These results suggests the importance of further experimental work to determine conditions for optimal H_2O_2 production that may occur at lower discharge power.

Because of the nature of the power supply used in the present work, we could not extend these experimental regions and this suggests where further work is needed.

Figure 17 shows the average rates of H_2O_2 degradation (determined from the reaction model) under different discharge powers. According to the results, the H_2O_2 degradation is much more significant in the argon plasma than in the helium plasma due to the higher electron density

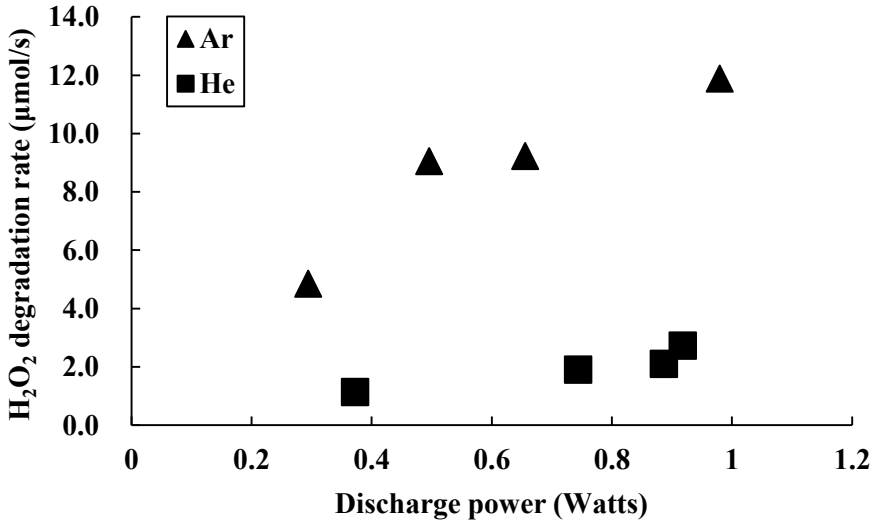

Fig 17. H_2O_2 degradation rates under different discharge power estimated from the reaction model described in Appendix I for each experimental condition of input discharge power. The error bars are within the size of the symbols due to the small variation of model input parameters.

and gas temperature. Figure 18 shows the calculated relative H_2O_2 degradation rate constants due to the reactions with electrons and ·OH in both argon and helium plasmas. In argon, the electron degradation predominates over ·OH based degradation in the range of discharge power considered and while the role of electrons drops with increasing power, the role of ·OH on degradation appears to slightly increase and then decrease. In the case of helium, degradation by ·OH predominates over most of the range of discharge power, however, as the power increases the relative roles of electron and ·OH have opposite trends. The magnitude of the electron collision rate constants are approximately 10 times larger in argon (due to the higher electron densities), but the total degradation rate constants are about a factor of 5 higher than the corresponding values in helium. The formation rate constants in argon are about a factor of 2.4 higher than in helium, thus indicating that the higher rates of formation in argon are balanced by correspondingly larger rates of degradation.

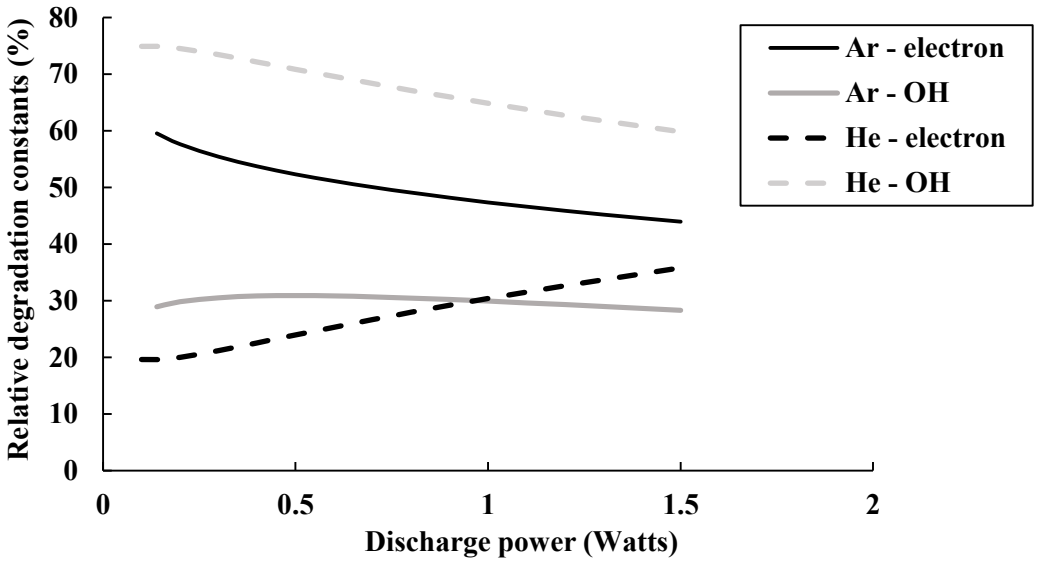

Fig 18. Model estimates of the relative roles of electron and hydroxyl radical reaction rates on H_2O_2 degradation for argon and helium cases with changes in discharge power. For OH: $(k_6C^o_{OH}/k_d')$ and for electrons $(k_7+ k_8+ k_9+ k_{10})C_e/k_d')$

Table 3 summarizes additional results from the model and experiments. While the concentration of ·OH is about 2 times higher in the argon than helium plasma, since the volume of the helium film is larger, the total amount of ·OH in the helium plasma is about double that in the argon plasma leading to higher energy yields in helium. In general, according to the simulation results, there are three reasons that lead to the slightly lower production rate of H_2O_2 in the argon discharge: firstly, the ·OH was not efficiently generated in argon discharge even though it has a much higher electron density; secondly, the ·OH didn't efficiently recombine to form H_2O_2; thirdly, the degradation of H_2O_2 was higher in the argon plasma due to higher densities of electrons and ·OH.

Table 3. Summary of key model and experimental results.

	Units	Argon	Helium	Ratio
From model				
$<C_{OH}>$	cm^{-3}	$3.9\text{-}4.8 \times 10^{14}$	$2.0\text{-}2.4 \times 10^{14}$	1.9-2.1
C_{OH}^{0}	cm^{-3}	$9.8\text{-}12.1 \times 10^{18}$	$5.0\text{-}6.0 \times 10^{18}$	1.8-2.1
OH total	molecules	$2.1\text{-}4.9 \times 10^{13}$	$4.2\text{-}6.2 \times 10^{13}$	0.5-0.7
Energy Yield (OH)	% (of 2×10^{-6} mole/J maximum limit)	12.0-8.3	18.6-11.3	0.7-0.8
V_{plasma}	cm^3	$0.9\text{-}3.3 \times 10^{-4}$	$1.4\text{-}2.2 \times 10^{-3}$	0.09-0.12
V_{film}	cm^3	$2.2\text{-}4.1 \times 10^{-6}$	$8.4\text{-}10.4 \times 10^{-6}$	0.30 – 0.35
From data				
P_{H2O2}	moles/s	$1.95\text{-}3.54 \times 10^{-8}$	$2.71\text{-}4.85 \times 10^{-8}$	0.7
H_2O_2 *Energy Yield*	g/kWhr	8.1-4.4	8.9-6.5	0.9—0.7
n_e	cm^{-3}	$1.8\text{-}2.0 \times 10^{16}$	$1.3\text{-}2.3 \times 10^{15}$	14-8

CONCLUSION

In this work, both argon and helium were used as the carrier gas to generate a nanosecond pulsed plasma discharge in a water film plasma reactor. The discharge power, plasma properties and diffuseness, and the H_2O_2 production rate and energy yield were measured and compared for plasmas generated in both argon and helium. It was found that the helium plasma is more diffusive as indicated by a larger volume with corresponding lower electron density and gas temperature. The diffuseness of the plasma was changed by increasing the helium percentage in the argon-helium gas mixture.

The H_2O_2 production rate increased with the discharge power in both the argon plasma and the helium plasma, and the H_2O_2 production rate was slightly higher in the helium plasma than in the argon plasma. This is because the production of H_2O_2 not only depends on the electron density and concentration of ·OH, but also on the plasma volume and plasma-liquid interface. In general, the electron density of the plasma increased with increasing discharge power as the voltage setting on the power supply was increased, which enhanced the collisions between water molecules and electrons, therefore causing more ·OH formation due to the enhanced electron-water collisions. The volume expansion of the plasma with discharge power increased the interface film region at the boundary of the plasma and liquid. However, the energy yield of H_2O_2 decreases with discharge power in both plasmas despite its higher production rate.

The diffuseness of the plasma is reflected by the increase of the plasma volume (and volume of the interfacial film region where H_2O_2 is formed) and the decrease of the electron density and gas temperature. Therefore, a diffusive plasma may generate a lower ·OH concentration, but leads to a larger total amount of ·OH and provides conditions that lead to effective radical recombinations to form H_2O_2 with lower rates of degradation. The diffusive plasma has a lower specific energy density, which reduces the H_2O_2 destruction during the discharge. A mathematical model describing the H_2O_2 formation and degradation rates within a small film region surrounding the plasma core with time dependent radical and electron quenching predicts that the ·OH concentration is 2 times higher in the argon plasma than in the helium plasma but the total amount of ·OH in the helium is higher due to the larger film region. The model and

experimental data both suggest that higher energy yields of H_2O_2 can be achieved in both plasmas at lower power or specific energy density.

ACKNOWLEDGEMENTS

The authors would also like to thank Dr. Jan Voráč from Masaryk University in the Czech Republic for a very helpful instruction on estimating the gas temperature of the plasma with the two temperature fitting approach. The authors would additionaly like to acknowlege Kosuke Tachibana, Luke Raymond, and Ken Miller for their discussions and aid in electrical diagnostics in nanosecond discharges. This work was supported by NSF (CBET: 1702166) and Florida State University. Bruce Locke would also like to acknowledge support from the Fulbright Commission of the Czech Republic and Florida State University for support.

APPENDIX I – Model Description

A general mass balance for a given species, i, in the plasma channel can be given by

$$\frac{\partial C_i}{\partial t} = \nabla \cdot D_i \nabla C_i + R_i \tag{A.1}$$

Where C_i is the concentration, D_i the diffusion coefficient, and R_i the net rate of formation of the specific species. Under conditions of a nanosecond plasma (with pulse with of 20 ns), we can consider the relative importance of the diffusion and transient terms. In the case of electrons the length scale for diffusion ($l=(2D_it)^{1/2}$) in this time period is of order 100 μm while for H_2O_2 the diffusion length is approximately 1 μm (see Table A1 for parameters used). Therefore, it is reasonable to assume that during a single pulse there is limited exchange of molecular species with the ambient environment and the diffusion term in Equation (A.1) above can be neglected. Furthermore, since the length scale for diffusion of H_2O_2 is limited to about 1 μm, we will consider a small film region at the outer boundary of the plasma channel of 1 μm where the H_2O_2 is formed since in the core of the plasma the higher temperatures and amounts of electrons will degrade this species. The material balance on H_2O_2, assuming a general formation rate by ·OH recombination (rate constant k_f) and a lumped first order degradation term (rate constant k_d) is given by

$$\frac{dC_{H2O2}}{dt} = k_f C_{OH}^2 - k_d C_{H2O2} \tag{A.2}$$

Since the time scale for decay of the plasma is very fast (see Figure 3 of main text) we will assume that the concentration of ·OH decays exponentially by

$$C_{OH} = C_{OH}^0 e^{-bt} \tag{A.3}$$

Where 1/b is the time constant for decay of order 5 ns based upon Figure 3 and C_{OH}^0 is the concentration of ·OH in the plasma film at the end of the pulse and is taken here as a fitting parameter. Since the degradation of H_2O_2 occurs by both radical (·OH, ·H, O) and electron reactions (see Table 2 in the main text) we will assume that the rate constant for H_2O_2 degradation follows the same trend as for ·OH concentration.

$$k_d = k_d' e^{-bt} \tag{A.4}$$

Therefore, Equation (A.2) becomes

$$\frac{dC_{H2O2}}{dt} = k'_f e^{-2bt} - k'_d e^{-bt} C_{H2O2} \tag{A.5}$$

If we assume that the initial state contains no H_2O_2, solution of Equation (A.5) gives

$$C_{H2O2} = k'_f \left\{ \frac{e^{-2bt}}{k'_d e^{-bt} - 2b} - \frac{exp\left((e^{-bt}-1)k'_d/b\right)}{k'_d - 2b} \right\} \tag{A.6}$$

For $t >> b$, Equation (A.6) reduces to

$$C_{H2O2} = k'_f / b \left\{ \frac{e^{-k'_d/b}}{2 - k'_d/b} \right\} \tag{A.7}$$

The amount of H_2O_2 present in the film region at the end of the pulse can be used to determine the production rate, P_{H2O2}, of H_2O_2 by

$$P_{H2O2} = C_{H2O2} V_{film} f \tag{A.8}$$

Where f is the pulse frequency. The volume of the film is determined by

$$V_{film} = L\pi\left(R_p^2 - (R_p - l)^2\right) \tag{A.9}$$

Where R_p is the plasma radius as measured, L the length of the plasma channel, and l the film thickness. The film thickness, here based upon diffusion length as mentioned above, of 1 μm is quite consistent with the measured mass transfer coefficient [6] which in turn also compares well with the literature for convective boiling by Reynolds analogy [6, 44].

Table A.1. Model input parameters.

Symbol	Property	Units	Source
P_w	Discharge power	Watts	Measured
n_e	Electron density	cm^{-3}	Measured
T_p	Plasma gas temperature	K	Measured
R_p	Plasma radius	cm	Measured, calculated

L	Plasma length (assumed equal to electrode gap distance)	cm	Designed
f	Pulse frequency	Hz	Setting
P_{H2O2}	H_2O_2 production rate	moles/s	Measured

Table A.2. Model parameters.

Symbol	Property	Units	Value	Source
P	Gas pressure	atm	2.5	[5]
D_e	Electron diffusion coefficient	cm^2/s	Ar: 520	Bolsigplus
			He: 1371	Bolsigplus
D_{H2O2}	H_2O_2 diffusion coefficient	cm^2/s	Ar(600K, 2.5 atm): 0.187	Chapman Enskog
			He(350 K, 2.5atm): 0.238	

The values for k_f' and k_d' used in the model, given in equations (A.10) (A.11), and (A.12), are determined from the functions given in Table 2 in the main text following the same assumption used by Du et al. [9]. For reactions 3 through 6 the radical densities are assumed equal (C_H=C_{OH}^0=C_O). The electron collision rates use the measured electron densities. The concentrations of argon and helium are determined with the ideal gas law using the measured temperature and 2.5 atm pressure.

$$k_d' = C_H(k_3 + k_4) + C_O k_5 + C_{OH}^0 k_6 + n_e(k_7 + k_8 + k_9 + k_{10}) \quad \text{(A.10)}$$

$$k_{f-argon}' = C_{Ar}(k_1)(C_{OH}^0)^2 \quad \text{(A.11)}$$

$$k_{f-helium}' = C_{He}(k_2)(C_{OH}^0)^2 \quad \text{(A.12)}$$

The model is fit to the experimental data for Ar and He using the C_{OH}^0 as the only fitting parameter with the measured values of n_e, T_p, and R_p. Once the values of C_{OH}^0 were determined

empirical functions were developed (see figures A1, A2, A3, and Figure 13) for C_{OH}^{0}, n_e, R_p and T_p (Argon) with discharge power, and the model was then used to predict the expected energy yields for H_2O_2 for power above and below the ranges of experimental data (see Figure 14).

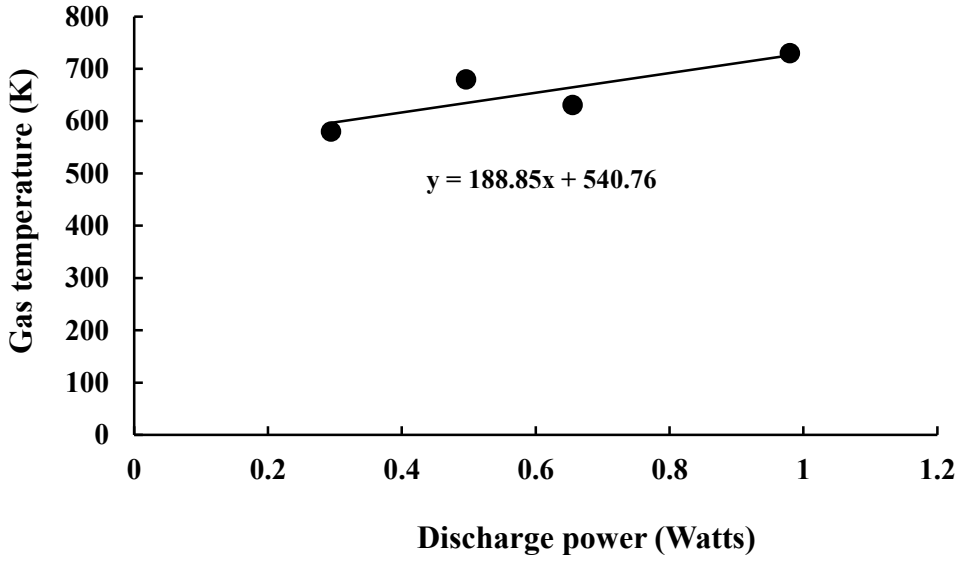

Fig. A.1. Experimental temperature for argon plasma fit to function with discharge power.

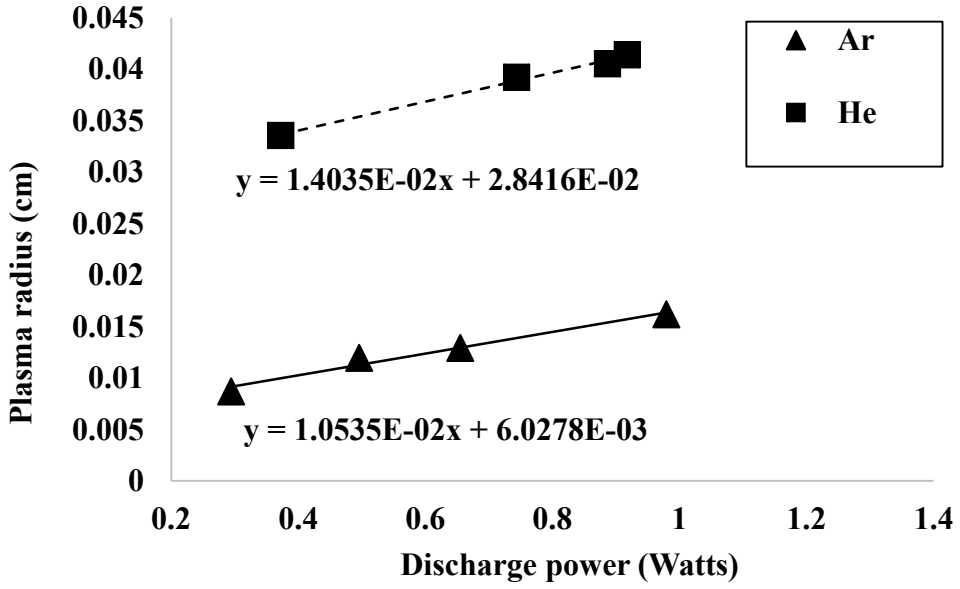

Fig. A.2 Plasma radius fit to linear functions for argon and helium.

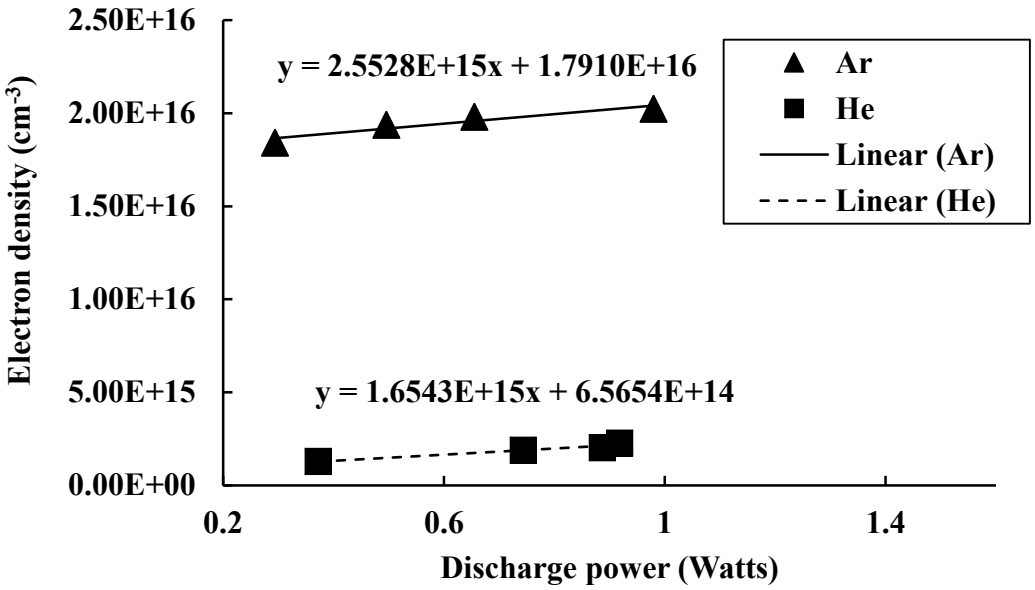

Fig. A.3 Experimental data on electron density fit to linear functions for argon and helium.

References:

[1] Locke B, Sato M, Sunka P, Hoffmann M and Chang J 2006 Electrohydraulic discharge and nonthermal plasma for water treatment *Industrial & Engineering Chemistry Research* **45** 882-905

[2] Bruggeman P and Leys C 2009 Non-thermal plasmas in and in contact with liquids *Journal of Physics D-Applied Physics* **42**

[3] Bruggeman P J, Kushner M J, Locke B R, Gardeniers J G E, Graham W G, Graves D B, Hofman-Caris R C H M, Maric D, Reid J P, Ceriani E, Rivas D F, Foster J E, Garrick S C, Gorbanev Y, Hamaguchi S, Iza F, Jablonowski H, Klimova E, Kolb J, Krcma F, Lukes P, Machala Z, Marinov I, Mariotti D, Thagard S M, Minakata D, Neyts E C, Pawlat J, Petrovic Z L, Pflieger R, Reuter S, Schram D C, Schröter S, Shiraiwa M, Tarabová B, Tsai P A, Verlet J R R, Woedtke T v, Wilson K R, Yasui K and Zvereva G 2016 Plasma–liquid interactions: a review and roadmap *Plasma Sources Science and Technology* **25** 053002

[4] Locke B R and Shih K Y 2011 Review of the methods to form hydrogen peroxide in electrical discharge plasma with liquid water *Plasma Sources Science & Technology* **20**

[5] Wandell R J, Wang H, Tachibana K, Makled B and Locke B R Nanosecond Pulsed Plasma Discharge over a Flowing Water Film: Characterization of Electrical and Plasma Properties and their Effect on Hydrogen Peroxide Generation *to be submitted to "Plasma Processes and Polymers"*

[6] Hsieh K C, Wandell R J, Bresch S and Locke B R 2017 Analysis of hydroxyl radical formation in a gas-liquid electrical discharge plasma reactor utilizing liquid and gaseous radical scavengers *Plasma Processes and Polymers* **14** 14

[7] Hofmann S, van Gessel A F H, Verreycken T and Bruggeman P 2011 Power dissipation, gas temperatures and electron densities of cold atmospheric pressure helium and argon RF plasma jets *Plasma Sources Science & Technology* **20**

[8] Hofmann S, Sobota A and Bruggeman P 2012 Transitions Between and Control of Guided and Branching Streamers in DC Nanosecond Pulsed Excited Plasma Jets *Ieee Transactions on Plasma Science* **40** 2888-99

[9] Du Y J, Nayak G, Oinuma G, Peng Z M and Bruggeman P J 2017 Effect of water vapor on plasma morphology, OH and H2O2 production in He and Ar atmospheric pressure dielectric barrier discharges *Journal Of Physics D-Applied Physics* **50**

[10] Iza F, Kim G J, Lee S M, Lee J K, Walsh J L, Zhang Y T and Kong M G 2008 Microplasmas: Sources, particle kinetics, and biomedical applications *Plasma Processes And Polymers* **5** 322-44

[11] Laroussi M 2009 Low-Temperature Plasmas for Medicine? *Ieee Transactions on Plasma Science* **37** 714-25

[12] Hsieh K C, Wang H and Locke B R 2016 Analysis of Electrical Discharge Plasma in a Gas-Liquid Flow Reactor Using Optical Emission Spectroscopy and the Formation of Hydrogen Peroxide *Plasma Processes and Polymers* **13** 908-17

[13] Wandell R J and Locke B R 2014 Hydrogen Peroxide Generation in Low Power Pulsed Water Spray Plasma Reactors *Industrial & Engineering Chemistry Research* **53** 609-18

[14] Eisenberg G M 1943 Colorimetric determination of hydrogen peroxide *Industrial And Engineering Chemistry-Analytical Edition* **15** 327-8

[15] Wandell R J and Locke B R 2014 Low-Power Pulsed Plasma Discharge in a Water Film Reactor *Ieee Transactions on Plasma Science* **42** 2634-5

[16] Bruggeman P J, Sadeghi N, Schram D C and Linss V 2014 Gas temperature determination from rotational lines in non-equilibrium plasmas: a review *Plasma Sources Science and Technology* **23** 023001

[17] Laux C 2002 Radiation and nonequilibrium collisional-radiative models *Physico-chemical modeling of high enthalpy and plasma flows* 2002-07

[18] Peter B, Daan S, Manuel Á G, Robby R, Michael G K and Christophe L 2009 Characterization of a direct dc-excited discharge in water by optical emission spectroscopy *Plasma Sources Science and Technology* **18** 025017

[19] Vorac J, Synek P, Prochazka V and Hoder T 2017 State-by-state emission spectra fitting for non-equilibrium plasmas: OH spectra of surface barrier discharge at argon/water interface *Journal Of Physics D-Applied Physics* **50**

[20] Nikiforov A Y, Leys C, Gonzalez M A and Walsh J L 2015 Electron density measurement in atmospheric pressure plasma jets: Stark broadening of hydrogenated and non-hydrogenated lines *Plasma Sources Science & Technology* **24**
[21] Hagelaar G and Pitchford L 2005 Solving the Boltzmann equation to obtain electron transport coefficients and rate coefficients for fluid models *Plasma Sources Science and Technology* **14** 722
[22] Moon S Y, Han J W and Choe W 2006 Control of radio-frequency atmospheric pressure argon plasma characteristics by helium gas mixing *Physics Of Plasmas* **13**
[23] Schroter S, Pothiraja R, Awakowicz P, Bibinov N, Boke M, Niermann B and Winter J 2013 Time-resolved characterization of a filamentary argon discharge at atmospheric pressure in a capillary using emission and absorption spectroscopy *J Phys D Appl Phys* **46**
[24] Wang Q, Doll F, Donnelly V M, Economou D J, Sadeghi N and Franz G F 2007 Experimental and theoretical study of the effect of gas flow on gas temperature in an atmospheric pressure microplasma *J Phys D Appl Phys* **40** 4202-11
[25] Ellis H, Pai R, McDaniel E, Mason E and Viehland L 1976 Transport properties of gaseous ions over a wide energy range *Atomic Data and Nuclear Data Tables* **17** 177-210
[26] Lieberman M A and Lichtenberg A J 2005 *Principles of plasma discharges and materials processing*: Hoboken, N.J. : Wiley-Interscience, 2005. 2nd ed.)
[27] Dobrynin D, Seepersad Y, Pekker M, Shneider M, Friedman G and Fridman A 2013 Non-equilibrium nanosecond-pulsed plasma generation in the liquid phase (water, PDMS) without bubbles: fast imaging, spectroscopy and leader-type model *Journal Of Physics D-Applied Physics* **46**
[28] Li D, Nikiforov A, Britun N, Snyders R, Kong M G and Leys C 2016 OH radical production in an atmospheric pressure surface micro-discharge array *Journal of Physics D-Applied Physics* **49**
[29] Simeni Simeni M, Roettgen A, Petrishchev V, Frederickson K and Adamovich I V 2016 Electron density and electron temperature measurements in nanosecond pulse discharges over liquid water surface *Plasma Sources Science Technology* **25** 064005
[30] Liu D X, Sun B W, Iza F, Xu D H, Wang X H, Rong M Z and Kong M G 2017 Main species and chemical pathways in cold atmospheric-pressure Ar + H2O plasmas *Plasma Sources Science & Technology* **26**
[31] Liu D X, Bruggeman P, Iza F, Rong M Z and Kong M G 2010 Global model of low-temperature atmospheric-pressure He + H2O plasmas *Plasma Sources Science & Technology* **19**
[32] Biondi M A and Chanin L M 1961 Blanc's law—ion mobilities in helium-neon mixtures *Physical Review* **122** 843
[33] Hsieh K C, Wandell R J, Bresch S and Locke B R 2017 Analysis of hydroxyl radical formation in a gas-liquid electrical discharge plasma reactor utilizing liquid and gaseous radical scavengers *Plasma Processes And Polymers* **14**
[34] Lindsay A, Anderson C, Slikboer E, Shannon S and Graves D 2015 Momentum, heat, and neutral mass transport in convective atmospheric pressure plasma-liquid systems and implications for aqueous targets *Journal of Physics D: Applied Physics* **48** 424007
[35] Tochikubo F, Uchida S and Watanabe T 2004 Study on decay characteristics of OH radical density in pulsed discharge in Ar/H2O *Japanese journal of applied physics* **43** 315
[36] Forster R, Frost M, Fulle D, Hamann H, Hippler H, Schlepegrell A and Troe J 1995 High pressure range of the addition of HO to HO, NO, NO2, and CO. I. Saturated laser induced fluorescence measurements at 298 K *The Journal of chemical physics* **103** 2949-58
[37] Atkinson R, Baulch D, Cox R, Crowley J, Hampson R, Hynes R, Jenkin M, Rossi M, Troe J and Wallington T 2008 Evaluated kinetic and photochemical data for atmospheric chemistry: Volume IV–gas phase reactions of organic halogen species *Atmospheric chemistry and physics* **8** 4141-496
[38] Baulch D, Cobos C, Cox R, Frank P, Hayman G, Just T, Kerr J, Murrells T, Pilling M and Troe J 1994 Evaluated kinetic data for combustion modeling. Supplement I *Journal of Physical and Chemical Reference Data* **23** 847-8
[39] Nandi D, Krishnakumar E, Rosa A, Schmidt W-F and Illenberger E 2003 Dissociative electron attachment to H 2 O 2: a very effective source for OH and OH− generation *Chemical physics letters* **373** 454-9

[40] Soloshenko I, Tsiolko V, Khomich V, Bazhenov V Y, Ryabtsev A, Schedrin A and Mikhno I 2002 Features of sterilization using low-pressure DC-discharge hydrogen-peroxide plasma *IEEE transactions on plasma science* **30** 1440-4
[41] Ono R 2016 Optical diagnostics of reactive species in atmospheric-pressure nonthermal plasma *Journal of Physics D-Applied Physics* **49**
[42] Winters C, Petrishchev V, Yin Z Y, Lempert W R and Adamovich I V 2015 Surface charge dynamics and OH and H number density distributions in near-surface nanosecond pulse discharges at a liquid / vapor interface *Journal of Physics D-Applied Physics* **48**
[43] Verreycken T, van der Horst R M, Baede A, Van Veldhuizen E M and Bruggeman P J 2012 Time and spatially resolved LIF of OH in a plasma filament in atmospheric pressure He-H2O *Journal of Physics D-Applied Physics* **45**
[44] Geankoplis C J 2003 *Transport Processes and Unit Operations*: Prentice Hall)